

DFT investigation of Ca mobility in reduced-perovskite and oxidized-marokite oxides

A. Torres^a, F.J. Luque^{b,c}, J. Tortajada^d, M.E. Arroyo-de Dompablo^{a,*}

^a Departamento de Química Inorgánica, Facultad de Ciencias Químicas, Universidad Complutense de Madrid, 28040, Madrid, Spain

^b Dpto. de Mineralogía y Petrología, Facultad de Geología, Universidad Complutense de Madrid, 28040 Madrid, Spain

^c Dpto. Geomateriales, Instituto de Geociencias IGE (CSIC, UCM), 28040, Madrid, Spain

^d Departamento de Química Física, Facultad de Ciencias Químicas, Universidad Complutense de Madrid, 28040, Madrid, Spain

ARTICLE INFO

Keywords:

CaMn₄O₈
Ca₂Fe₂O₅
Ca₂Mn₂O₅
Post-spinel
Calcium batteries

ABSTRACT

Progress in the development of rechargeable Ca-ion batteries demands the discovery of potential cathode materials. Transition metal oxides are interesting candidates due to their theoretical high energy densities, but with the drawback of a low Ca mobility. Previous computational/experimental investigations associate the electrochemical inactivity of various oxides (CaMO₃-perovskite, CaMn₂O₄-post-spinel and CaV₂O₅) to high energy barriers for Ca migration. The introduction of oxygen and/or Ca vacancies in ternary transition metal oxides is a likely way to reshape the local topology and hence improve the Ca diffusivity. In this work, the energy barriers for Ca migration are calculated and discussed for (i) oxygen-deficient perovskites within the related Ca₂Fe₂O₅-brownmillerite and Ca₂Mn₂O₅ structures, and (ii) tunnel CaMn₄O₈, a derivative of the CaMn₂O₄-marokite with Ca vacancies.

1. Introduction

High energy density electrochemical energy storage systems are urgently needed to satisfy the increasing demand for energy and power at lower costs. Rechargeable batteries based on the intercalation reaction of divalent cations (Ca²⁺, Mg²⁺) have been proposed as promising alternatives to Li-ion batteries [1,2]. Theoretically, rechargeable batteries based on a Ca metal anode could exhibit advantages in terms of energy density, safety and cost. In practice, however, the design of such batteries is difficultly by the lack of competitive electrode materials and electrolytes [3,4]. While recent research advances have shown that calcium can be plated and stripped in organic electrolytes [5,6], the identification of suitable cathode material is so far a pending issue [3,4,7]. Limited reversible electrochemical Ca intercalation has been reported for a handful of compounds (TiS₂ [8], MoO₃ [9], Ca_{0.5}CoO₂ [10], manganese hexacyanoferrate [2]), all of them showing poor cycling capability. The discovery of electrode materials can be accelerated using computational techniques. In particular, the utility of Density Functional Theory (DFT) methods to screen for potentially interesting positive electrode materials has been widely proven in the last two decades (see for instance Ref. [11] and references therein).

The relevant electrochemical characteristics of several ternary oxides

as cathode materials for rechargeable Ca batteries have been foreseen using DFT calculations [12–17]. The [Ca]_T[Mn₂]O₄ spinel and the δ-Ca_xV₂O₅ phases appear as promising electrode materials in terms of voltage, specific capacity and ionic diffusion [12,16,17]. However, these compounds can be regarded as virtual materials since they have never been obtained experimentally. In their crystal structures the Ca-sites have unusually low coordination with oxygen ions, and hence they are metastable compared to the known polymorphs where the Ca ions present the more stable eight-fold coordination (marokite-CaMn₂O₄ and α-Ca_xV₂O₅) [14,18]. Despite the interest of these virtual oxides, for the existing oxides CaMn₂O₄, CaMO₃, α-V₂O₅ and Ca-Co-O phases, parallel experimental-computational researches establish a link between the lack of reversible electrochemical activity (experimentally observable) and a limited Ca diffusion (computational prediction) [14,15,17,19,20]. Indeed, one of the major concerns in the cathode design for the divalent battery technology is the limited mobility of Mg²⁺ and Ca²⁺ ions in inorganic structures. The migration energy barriers, which can be extracted from DFT calculations, provide an approximate indication of the ionic diffusivity [21]. It has been estimated that for a reasonable cell power rate (discharging time 2 h) the energy barriers for cation diffusion should be below 0.525 eV in micrometer particles and 0.625 eV in nanosized-particles [16,17].

* Corresponding author.

E-mail address: e.arroyo@quim.ucm.es (M.E. Arroyo-de Dompablo).

<https://doi.org/10.1016/j.ensm.2019.06.002>

Received 31 December 2018; Received in revised form 31 March 2019; Accepted 2 June 2019

Available online xxxx

2405-8297/© 2019 The Authors. Published by Elsevier B.V. This is an open access article under the CC BY-NC-ND license (<http://creativecommons.org/licenses/by-nc-nd/4.0/>).

Factors controlling diffusion are based on crystal chemistry [16]. The existence of interconnected Ca sites forming migration pathways within the structure is a pre-requisite. The pathways should be wide enough for the Ca ion, and with a favorable topology to diminish the electrostatic interactions between the diffusing Ca^{2+} cation and the rest of chemical components in the structure. Therefore, compared to Li^+ diffusion, the handicap for Ca mobility resides in the larger size of Ca^{2+} ions on one hand, and its divalent charge on the other that increases the electrostatic repulsion/atraction with the neighbouring cations/anions in the structure. Although decoupling both factors unambiguously is not plausible, signatures of either charge- or size-driven limiting mobility can be inferred for some materials. For the size-effect, previous investigations found that the larger size of Ca ions is the bottleneck for diffusion in structures that otherwise allow the diffusion of the smaller Li and Mg ions. Good examples are the post-spinel phases AMn_2O_4 ($\text{A} = \text{Li}, \text{Na}, \text{Mg}, \text{Ca}$) [14,22]. In other structural types, the dominant factor seems to be the coulombic repulsion between the Ca^{2+} cations and the other cations in the structure. That is the case of the perovskite structure, where a high energy barrier for Ca mobility (2 eV) arises from the face-sharing between the transition metal (TM) octahedra and the empty sites available for Ca diffusion [7,15].

The ability of transition metal ions to adopt different oxidation states and coordination environments plays in favor of a “topology based design”. The local topology of many oxides changes in the related oxidized/reduced phases, and consequently introducing oxygen and/or Ca vacancies in ternary transition metal oxides may be a key factor for enhanced Ca mobility. To explore this possibility, this work presents a DFT investigation of Ca mobility in reduced-perovskite and oxidized-marokite structures. The energy barriers for Ca migration are calculated and discussed for (i) oxygen-deficient perovskites within the related

brownmillerite and $\text{Ca}_2\text{Mn}_2\text{O}_5$ structures, and (ii) tunnel CaMn_4O_8 , a derivative of the marokite $\text{Ca}_2\text{Mn}_2\text{O}_4$ with a lower Ca/Mn ratio. We will show that the incorporation of oxygen vacancies may substantially modify the electrode characteristics of the materials. In a wider context, this is in line with the enhanced electrochemical properties of oxygen-deficient perovskites (see for instance Refs. [23–28]).

2. Structures

Fig. 1a shows the ideal perovskite structure of CaMO_3 where M denotes the transition metal cation; it is built up from corner-sharing MO_6 octahedra and the Ca ions are twelve-fold coordinated by oxygen. Oxygen vacancies in the perovskite structure lead to the brownmillerite-type structure (**Fig. 1b**) with the general formula $\text{A}_2\text{M}_2\text{O}_5$. It can be described as an oxygen-deficient perovskite, where the oxygen vacancies are fully ordered, resulting in alternate layers of corner-sharing octahedra and tetrahedra parallel to (010) (Space Group $Pnma$) [29]. A transition to a cubic perovskite might occur at higher temperatures, in which vacancies become disordered [30]. The Ca ions are in irregular eight-corner polyhedra, with ten triangular and one quadrangular faces. While $\text{Ca}_2\text{Fe}_2\text{O}_5$ crystallizes in the brownmillerite structure, reduction of CaMn_3O_6 results in a different ordered oxygen deficient perovskite, $\text{Ca}_2\text{Mn}_2\text{O}_5$, in which each octahedron turns into a square-base pyramid [31,32]. Thus, the crystal structure of $\text{Ca}_2\text{Mn}_2\text{O}_5$ is built up by chains of five-coordinated Mn^{3+} cations with nearly square pyramidal coordination, forming a 3D framework (**Fig. 1c**) [33]. The manganese polyhedra form rings of six $[\text{MnO}_5]$ units in the *ab* plane linked to other rings by corner sharing. The Ca atoms fit in a ten-fold polyhedron with eight triangular faces and four quadrangular faces.

The structure of post-spinel (or marokite) CaMn_2O_4 is built up from

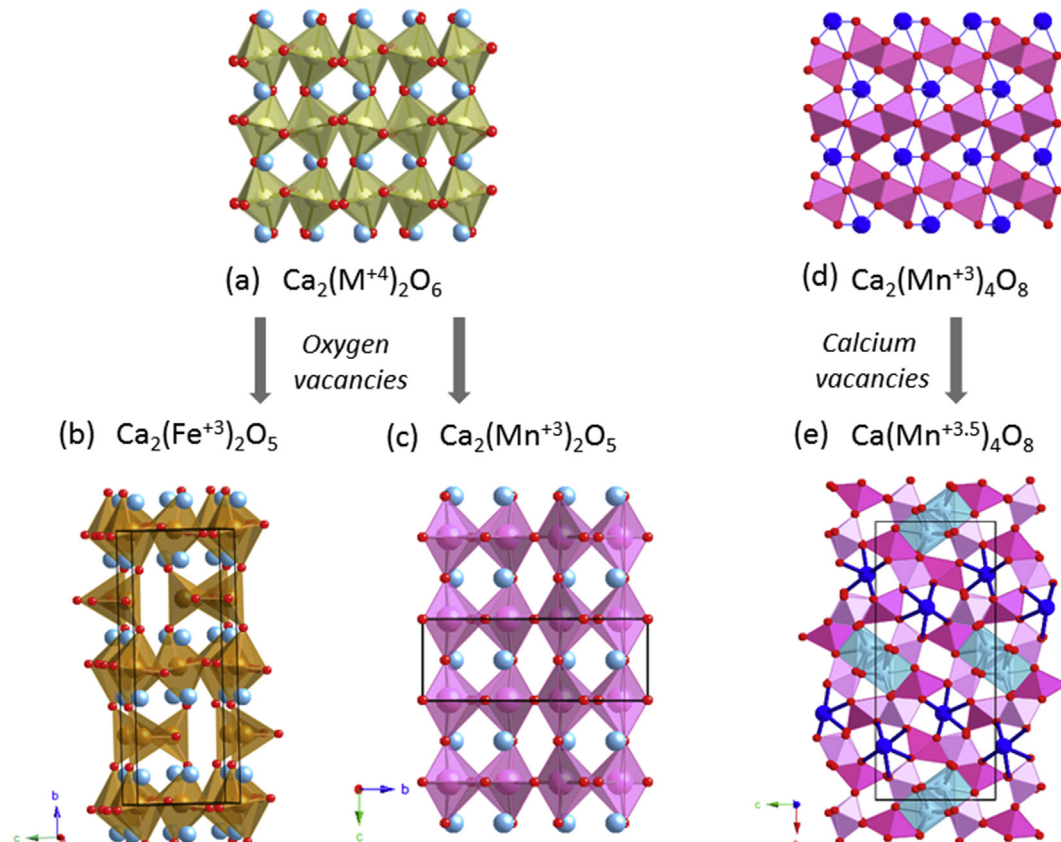


Fig. 1. Crystal structures of the investigated oxides. (a) perovskite CaMO_3 , (b) brownmillerite $\text{Ca}_2\text{Fe}_2\text{O}_5$, (c) $\text{Ca}_2\text{Mn}_2\text{O}_5$, (d) marokite- CaMn_2O_4 and (e) CaMn_4O_8 . Color code: Ca in blue, M (transition metal) in pale green, Fe in brown, Mn^{3+} in dark pink, Mn^{4+} in light pink, O in red. (For interpretation of the references to colour in this figure legend, the reader is referred to the Web version of this article.)

edge-sharing chains of MnO_6 octahedra, forming double rutile chains [34]. Each double-rutile chain is connected to two adjacent chains through edge-sharing oxygen and to another two chains through corner-sharing oxygen (see Fig. 1d). As a result, tunnels appear in the framework, where Ca ions occupy triangular prismatic sites with capped rectangular faces and Ca–O distances in the range 2.28–2.65 Å. The MnO_6 octahedron in the structure is distorted by the Jahn-Teller effect of octahedral Mn^{3+} in high spin configuration. Several authors have reported synthesis approaches to decrease the Ca concentration of marokite CaMn_2O_4 , leading to mixed $\text{Mn}^{4+}/\text{Mn}^{3+}$ oxides exhibiting interesting properties [35–37]. For a Ca:Mn atomic ratio equal to 1:4 (CaMn_4O_8) a tunnel structure is stabilized. The tunnel structure of CaMn_4O_8 can be at first described as a pure octahedral structure, with single and triple chains of edge-sharing MnO_6 octahedra, interconnected through the corners [38]. However, as illustrated in Fig. 1e, charge ordering produce a differentiation between half of the Mn ions in slightly distorted octahedra (Mn^{4+}, d^3 configuration) and half in a nearly five-fold coordination (Mn^{3+}, d^4 configuration). The $[\text{Mn}_4\text{O}_8]$ framework gives rise to three types of tunnels: empty rutile-like tunnels, six-sided (as those in the marokite) and eight-sided tunnels. The Ca^{2+} ions are situated in the six- and eight-sided tunnels, with half of the Ca sites being vacant. The Ca(1) ions (dark blue in Fig. 1e) inside the six-sided tunnels fit in a polyhedron similar to that in the marokite structure, with Ca(1)-O distances in the range 2.25–2.84 Å. The Ca(2) ions (light blue in Fig. 1e), located in the eight-sided tunnels, are surrounded by seven oxygen atoms forming a mono-capped triangular prismatic environment. The Ca(2)-O distances range from 2.15 to 2.55 Å.

3. Methodology

The calculations have been carried out using the ab-initio total-energy and molecular dynamics program VASP (Vienna ab-initio simulation program) developed at the Universität Wien [39]. Total energy calculations based on Density Functional Theory (DFT) were performed within the General Gradient Approximation (GGA), with the exchange and correlation functional form developed by Perdew, Burke and Ernzerhof (PBE) [40]. The interaction of core electrons with the nuclei is described by the Projector Augmented Wave (PAW) method [41]. The energy cut off for the plane wave basis set fix at a constant value of 600 eV throughout the calculations. The integration in the Brillouin zone is done on an appropriate set of k -points determined by the Monkhorst-Pack scheme. A convergence of the total energy close to 10 meV per formula unit is achieved with such parameters. A ferromagnetic configuration was selected in all cases. All crystal structures were fully relaxed (atomic positions, cell parameters and volume). The final energies of the optimized geometries were recalculated to correct the changes in the basis set of wave functions during relaxation. The initial atomic positions are taken from the reported structures of $\text{Ca}_2\text{Fe}_2\text{O}_5$ [29], $\text{Ca}_2\text{Mn}_2\text{O}_5$ [33] and CaMn_4O_8 [38]. In the latter, Ca occupied and vacant sites alternate in the tunnels.

Calcium mobility is investigated using the Nudged Elastic Band method (NEB) as implemented in VASP. To study diffusion, a vacancy is created in the structural model of the stoichiometric oxides and a simply jumping mechanism from an occupied position to the vacant site is considered. We used superstructures of the unit cells that guarantee a minimum interaction between defects: $\text{Ca}_{31}\text{Fe}_{32}\text{O}_{80}$ ($2 \times 1 \times 2$ of the unit cell), $\text{Ca}_{23}\text{Mn}_{24}\text{O}_{60}$ ($2 \times 1 \times 3$ of the unit cell) and $\text{Ca}_{15}\text{Mn}_{64}\text{O}_{128}$ ($1 \times 2 \times 1$ of the unit cell). Constant volume calculations were performed within the GGA approximation for three or five intermediate images initialized by linear interpolation between the two fully relaxed end-points. To converge the minimum energy path in the NEB procedure, the convergence threshold of the total energy of each image was set to 1×10^{-4} eV, with a residual force threshold of 0.01 eV/Å. To calculate the energy at the saddle point, cubic splines were fit through the relaxed images along each hop.

Average voltage for Ca deinsertion from $\text{Ca}_2\text{Fe}_2\text{O}_5$ ($\text{Fe}^{3+}/\text{Fe}^{4+}$ redox

couple) was calculated within the GGA + U method, following the methodology described by Aydinol et al. [42]. For consistency with the literature on this topic [12,15,16,43], the effective U value for the Fe-d orbitals were set to 5 eV ($J = 1$ eV).

4. Results

$\text{Ca}_2\text{Fe}_2\text{O}_5$. In the brownmillerite structure, the interconnected Ca sites form a channel along the b -axis (see Fig. 1b). The calculated energy barrier along this channel is 2.3 eV (Fig. 2a), similar to the predicted for the perovskite structure (around 2 eV) [15]. This is not surprising, since diffusion along this pathway involves Ca jumps between sites with the same topology than in the perovskite structure. Diffusion in the ac plane, consisting of tetrahedral $[\text{FeO}_4]$ units, is possible along the pathway shown in Fig. 2b: the oxygen vacancies respective to the perovskite structure create a zigzag path for potential Ca motion. As shown in Fig. 2b and c the initial and final Ca sites share triangular faces, being connected through an interstitial site that does not share any face with the FeO polyhedra. This contrasts with the perovskite structure, where the interstitial site shares faces with the FeO octahedra. The direct interpolation of three images between the relaxed end-points favors the path out from the Ca-Ca shared triangular face, slightly above the O-O dumbbell bond (see Fig. 2c). At the saddle point, the Ca^{2+} adopts a three-fold coordination with Ca-O distances 2.22–2.31 Å to the O-O dumbbell and the apical oxygen. The Ca-Fe distances are 2.84 Å and 3.01 Å to the two adjacent Fe ions in tetrahedral coordination, and 3.10 Å to the two Fe ions in octahedral coordination in the plane below. Note that migration across the interstitial site avoiding the O-O dumbbell would result in too short Ca-tetrahedral Fe distances. The calculated energy barrier along this path is 1 eV; the transition state in the brownmillerite seems stabilized respecting the perovskite.

$\text{Ca}_2\text{Mn}_2\text{O}_5$. Fig. 3 shows the analysis of the Ca diffusion pathways in the $\text{Ca}_2\text{Mn}_2\text{O}_5$ structure. Along the c -axis, the neighbouring Ca ions share a triangular face forming a tunnel of interconnected Ca ions (Fig. 3a). The small size of the triangular face precludes Ca diffusion (Ca-O distances at the saddle point are 2.12, 2.18 and 2.22 Å). Consequently, the calculated energy barrier is 2.6 eV (Fig. 3b, pathway 1). In the ab plane, there are two different pathways (Fig. 3c). Along the pathway labelled as 2, the adjacent Ca sites share an edge, with the intermediate eight-fold coordination site sharing faces with the Mn-O polyhedra. If the Ca ion hops from the equilibrium position to this site, a large Coulombic repulsion is generated, because of the short distance between Ca^{2+} and Mn^{3+} ions. Therefore, the Ca ion is pushed to jump across the common edge between the two neighbouring CaO polyhedra (Ca-O distance 2.22 Å). The calculated energy migration barrier is 2.2 eV. The pathway denoted as 3 in Fig. 3c and d implicates inter-connected Ca sites sharing a quadrangular face. In the diffusion along this channel, the Ca ion passes across the square face with Ca-O distances of 1.95–2.26 Å. At the saddle point the Ca ion is in the middle of a square face sharing edges with the four Mn-O polyhedra (see Fig. 3d), with Ca-Mn distances 2.79 Å \times 2 and 2.88 Å \times 2. The calculated energy barrier is 1.8 eV.

CaMn_4O_8 . Fig. 1 shows the two types of Ca ions in this structure: Ca(1) in the six-sized tunnels and Ca(2) in eight-sized tunnel. The calculated energy differences to create a vacancy in the Ca(1) vs the Ca(2) sites (0.77 eV for $\text{Ca}_7\text{Mn}_{32}\text{O}_{64}$ and for 0.52 eV for $\text{Ca}_{15}\text{Mn}_{64}\text{O}_{128}$) suggest that Ca ions will preferably deintercalate from the Ca(2) sites in the eight-sized tunnels. In these tunnels, there are two possible diffusion pathways labelled as 1 and 2 in Fig. 4a. The topology of pathway 1 is similar to that in the marokite structure: a tunnel formed by triangular-face sharing interconnected Ca sites. In CaMn_4O_8 the distance between Ca ions is 5.78 Å, as there is a vacant Ca site in between. The Ca ion passes across a triangular face of the polyhedra to the intermediate vacant site that represents a local minimum in the energy landscape (Fig. 4b). The Ca-O distance in the triangular window are too short (Ca-O distances are 2.09, 2.20 and 2.25 Å), as also found in the marokite structure [14], and accordingly, the calculated energy barrier is similarly high (2.2 eV). In

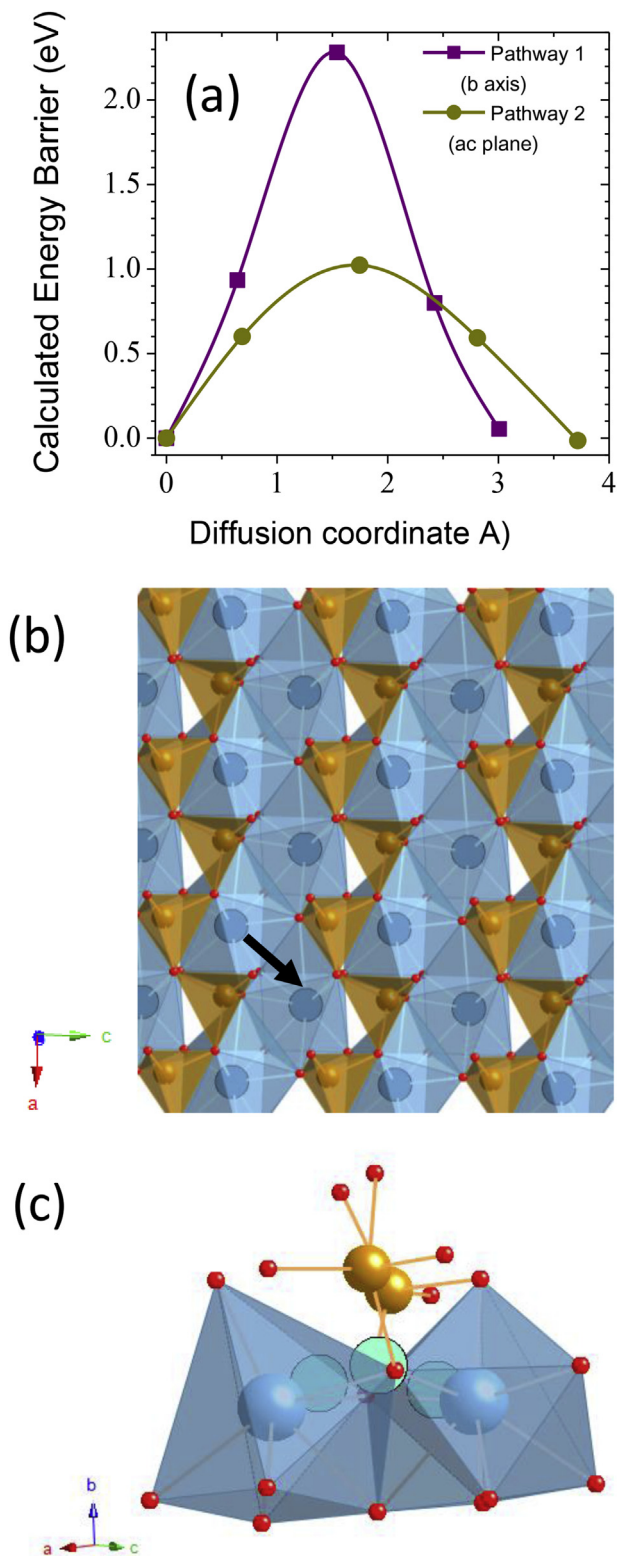


Fig. 2. (a) Calculated energy barrier for Ca diffusion in $\text{Ca}_2\text{Fe}_2\text{O}_5$. (b) Pathway along the ac plane. The arrow indicates the hopping mechanism from the occupied to the empty Ca sites. (c) Detail of the intermediate site along the diffusion pathway. Color code: Ca light blue, diffusing Ca in cyan, Fe brown, O red. (For interpretation of the references to colour in this figure legend, the reader is referred to the Web version of this article.)

pathway 2, the direct interpolation of three images between the relaxed end-points favors the path across the shared-edge of the two neighbouring Ca sites separated by 3.14 Å. In the transition state, the Ca^{2+} fits in the edge midway the O-O dumbbell ($\text{Ca}-\text{O}$ distance 2.05 Å), but with sufficiently large Ca–Mn distances of 3.31, 3.34 (x2) and 3.38 Å. Therefore, the high calculated energy barrier of 1.7 eV seems to be more related to size than to charge effects. This energy landscape is slightly asymmetric, with the energy of the start and end points differing in 0.17 eV. The orbital and $\text{Mn}^{3+}/\text{Mn}^{4+}$ charge ordering in CaMn_4O_8 [38] is disrupted due to the vacancy incorporation and such a complex electronic structure is difficult to capture with DFT approximations.

5. Discussion

The results for CaMn_4O_8 (path 1) indicate that the large size of Ca ions is an obstacle for Ca diffusion in marokite-related structures. Interestingly, tunnels of Ca ions sharing triangular faces exist in other structural types. Table 1 lists the calculated energy barriers for selected examples. In all cases, the migration barriers exceed 1.5 eV, independently on the Ca occupation of the tunnel; for a given tunnel, the incorporation of Ca vacancies does not lower the energy barriers (compare $\text{CaV}_2\text{O}_5/\alpha\text{-V}_2\text{O}_5$ and $\text{CaMn}_2\text{O}_4/\text{CaMn}_4\text{O}_8$). These results suggest that triangular-face tunnels are unfavorable for Ca^{2+} diffusion. This contrasts with the predicted diffusivity of Li^+ , Na^+ and Mg^{2+} in those tunnels (see Table 1). Importantly, the calculated energy barriers of Table 1 follow the order $\text{Li}^+ < \text{Mg}^{2+} < \text{Na}^+ < \text{Ca}^{2+}$, in consonance with both the ionic radii ($r_{(\text{VI})} = 0.76$ Å (Li^+), 0.72 Å (Mg^{2+}), 1.02 Å (Na^+), and 1.0 Å (Ca^{2+}) [44]) and the ionic charge. Since Ca^{2+} and Na^+ ions have comparable ionic radii, the larger barrier of the former calls for a size-charge join effect. In addition to the marokite structure (or CM) Table 1 lists the calculated energies for a second CaMn_2O_4 polymorph (denoted as CF). The CF and CM forms are known as post-spinel phases; they show very similar structures based on double-rutile chains, interconnected by vertex and edge sharing oxygen in CM but only through vertex sharing oxygen in CF. Noteworthy, the calculated energy barriers for the CF polymorph are substantially lower than those for the CM-polymorph (marokite). This reinforce the role of the electrostatic interactions in the energy barriers.

Standing on size arguments, structures with Ca-diffusion pathways consisting of triangular faces of low-coordination polyhedra, or quadrangular windows of large-coordination polyhedra, seem more adequate for Ca mobility. In the lowest energy pathway of the $\text{Ca}_2\text{Mn}_2\text{O}_5$ structure (pathway 2 in Fig. 4), the adjacent Ca sites share a quadrangular face of the ten-fold polyhedra. The larger size of this face favors Ca mobility. Nevertheless, at the transition state the channel shares the four edges with the surrounding Mn polyhedra, with the electrostatic repulsions raising the energy of the intermediate site to 1.8 eV. This points out to the energy landscape for Ca motion being rather charge-than size-limited, similarly to the case of the perovskite structure.

In the brownmillerite structure of $\text{Ca}_2\text{Fe}_2\text{O}_5$, the oxygen vacancies create a new pathway, with the diffusing Ca ion hopping slightly above the O-O dumbbell of the edge-shared between adjacent Ca sites. Hence, there is a size-penalty, with the energy of the first image from the pathway being quite high (0.6 eV). In turn, at the transition state, the Ca ion has no face-sharing with the Fe polyhedra, being the closer Fe ions at distances of around 3 Å. The weaker electrostatic repulsions in brownmillerite, compared to the perovskite structure or the CaMn_2O_5 structures, lowers the calculate energy barrier down to 1 eV. The substantial dropping from 2 eV in the perovskite to 1 eV in the brownmillerite is not enough to propose the latter as electrode material. For completeness, we have calculated the average voltage for Ca deinsertion according with the reaction:



Ca deinsertion involves the $\text{Fe}^{3+}/\text{Fe}^{4+}$ couple, with a theoretical specific capacity of 198 mAh/g. The predicted voltage (4.16 V) is beyond

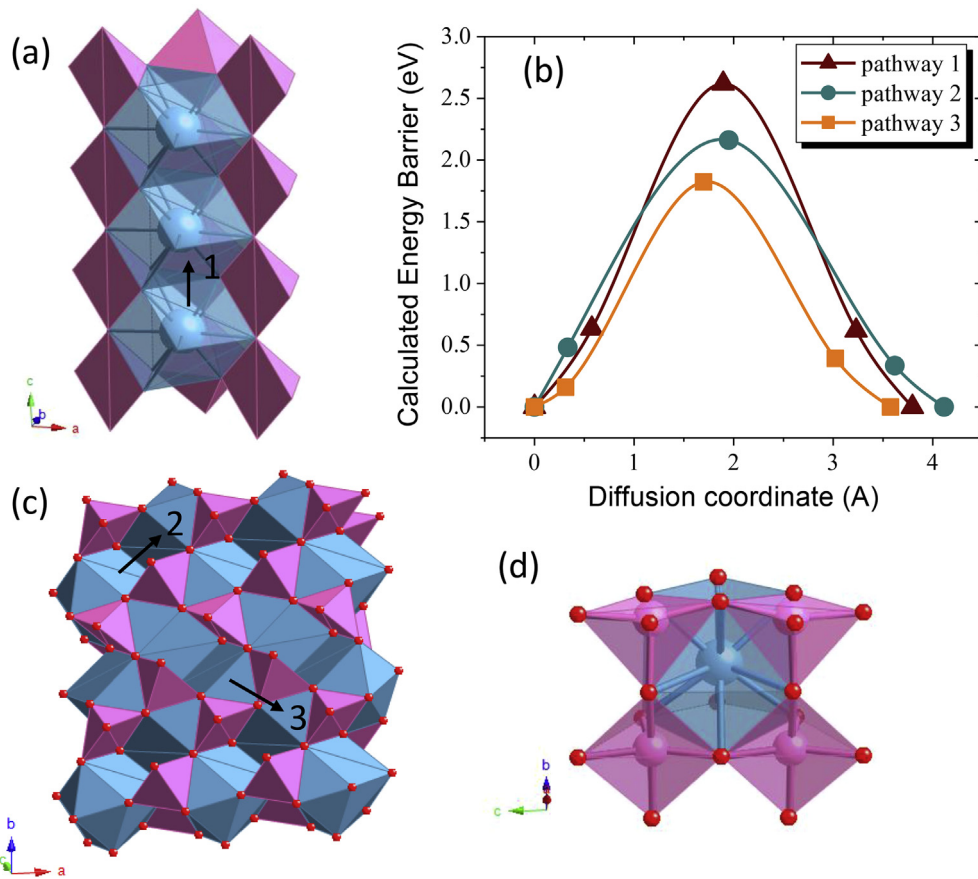


Fig. 3. Analysis of Ca mobility in $\text{Ca}_2\text{Mn}_2\text{O}_5$. (a) View of the pathway along the c axis. (b) Calculated energy barriers for paths 1–3. (c) The two possible pathways in the ab plane. (d) View of the most favorable pathway 3, showing the quadrangular window at the transition state. Color code: Ca in blue, Mn in pink, O in red. (For interpretation of the references to colour in this figure legend, the reader is referred to the Web version of this article.)

the stability window of the current electrolytes [5,7], making inviable the experimental investigation of $\text{Ca}_2\text{Fe}_2\text{O}_4$ as cathode material at the current state of the Ca batteries technology.

Enhancing the Ca mobility in oxides is a tricky crystal design challenge. Anion-deficient oxides occur commonly and, in cases where the anions are ordered, a variety of complex structures with reduced TM coordination number are generated. As a rule of thumb, creating a sufficient amount of ordered oxygen vacancies assists to reduce the face-sharing polyhedra between the Ca and TM sublattices. Even though this route allows weakening the Coulombic interactions, the aforementioned size issue constrains the candidate structures to those with Ca ions in polyhedra entailing large faces. Actually, a low Ca energy barrier (0.5 eV) has been reported for the virtual and metastable spinel $\text{Ca}_T[\text{Mn}_2]\text{O}_4$ [12], in which Ca ions occupies tetrahedral sites that have larger triangular faces than higher-coordination number polyhedra. The alternatives are stable structures based on Ca-highly coordinated oxygen polyhedra, but possessing quadrangular faces. Structures of reduced perovskites, such as $\text{Sr}_4\text{Fe}_4\text{O}_{11}$ might fulfill these requirements [45]. Ca-exchanged layered-perovskites belonging to the Ruddlesden-Popper and the Dion-Jacobson series are other interesting oxides to explore [46].

Note that in this work the barriers for Ca migration were assessed in the low-vacancy regime, since the investigated materials are synthesizable in their discharged state. The concentration of Ca in the host material varies along the charge of the cell, thereby affecting the migration barriers. Table 1 listed some example of materials with a subtle implication of Ca concentration in the energy barriers, as the main bottleneck in these structures is the narrow size of the tunnel for Ca diffusion. It should however be highlighted that this is not a general rule. Ca deintercalation might enhance the electrostatic repulsions (more oxidized TM

cations), raising the energy barriers for Ca migration. This effect is more significant for the multivalent ions. For instance, the calculated energy barrier for Mg migration in olivine- $\text{Mg}_x\text{MnSiO}_4$ spans in a 0.7 eV range (0.8 eV at $x = 1$, 1.5 eV at $x = 0.5$ and 1.3 eV at $x = 0$) [43], whereas the variation in olivine- Li_xMnPO_4 is only 0.08 eV (0.25 eV at $x = 1$ and 0.33 eV at $x = 0$) [21]. In this regard, additional DFT investigation and parallel experimental research in electrochemically active Ca cathodes (such as TiS_2 [8], MoO_3 [9] or $\text{Ca}_3\text{Co}_2\text{O}_6$ [20]) are necessary to advance in the field.

6. Conclusions

Transition metal oxides are a major class of compounds displaying a variety of crystal structures. By tuning the oxidation state of the transition metal, related structural types based on different TM polyhedra, or polyhedra arrangements, are accessible. The DFT results evidence that for some of these oxidized/reduced oxides the Ca mobility is equally hampered than in the parent oxides (i.e. CaMn_4O_8 or $\text{Ca}_2\text{Mn}_2\text{O}_5$), due to the occurrence of Ca sites with small triangular faces. A second key factor is to forestall the face sharing between the TM polyhedra and the Ca-intermediate site. DFT results reveal that this can be accomplished in some reduced oxides (i.e. $\text{Ca}_2\text{Fe}_2\text{O}_5$ versus CaFeO_3). Computational research is ongoing to pinpoint structures satisfying the topological criteria for Ca mobility. Oxygen-deficient oxides of the abundant and affordable Mn and Fe ions are worthy of attention.

It should be underlined that, despite the effectiveness of using DFT methods as a constructive instrument in the quest for Ca ion conducting materials, experimental advances concerning electrolytes and testing protocols are critical to confirm the suitability of DFT-proposed materials

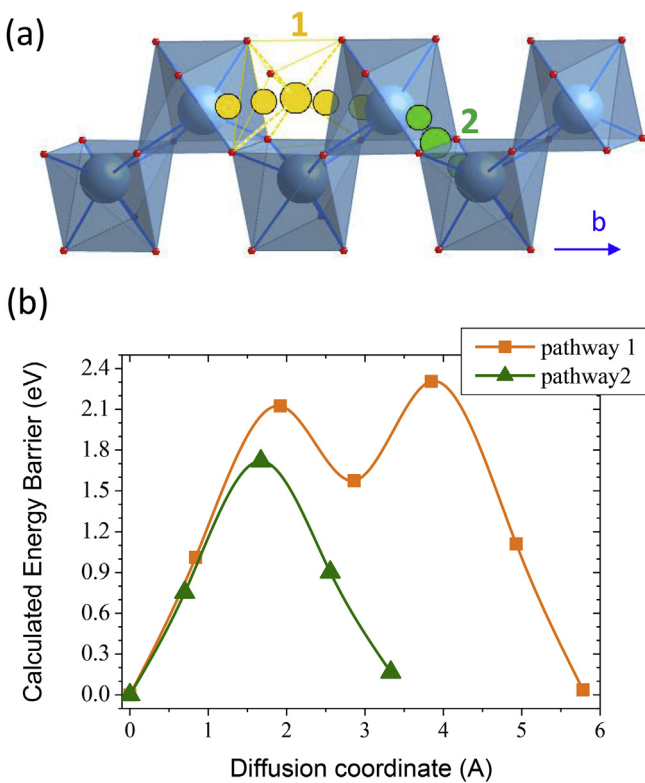


Fig. 4. (a) View of the Ca diffusion pathways in the eight-sided channels of CaMn_4O_8 . (b) Calculated energy barriers for Ca diffusion in CaMn_4O_8 .

Table 1

Calculated energy barriers for Ca diffusion in tunnels formed by triangular face sharing sites. For comparison, the calculated energy barriers for other intercalants are listed when available.

| Compound | n-fold of the Ca polyhedra | Ca occupancy | Calculated Ca energy barrier (eV) | Calculated energy barriers for other intercalants (eV) |
|---|----------------------------|--------------|-----------------------------------|---|
| Marokite- CaMn_2O_4 (CM structure) | 8 | 1 | 1.8 [14] | Li: 0.3 [22] Na: 1 [22] Mg: 0.75 [22] |
| CaMn_4O_8 (eight sided- tunnel) | 7 | 1/2 | 1.7 [this work] | |
| CaMn_2O_4 (CF structure) | 8 | 1 | 1.3 [14] | Li: 0.1 [22] Na: 0.38 [22] Mg: 0.4 [22] |
| CaV_2O_5 | 8 | 1 | 1.6 [this work] 1.9 [17] | |
| $\alpha\text{-V}_2\text{O}_5$ | 8 | 0 | 1.7 [17] 1.8 [47] | Li: 0.31 [47], 0.3 [17] Na: 1.16 [47] Mg: 0.97 [47], 0.9 [17] |
| $\text{Ca}_2\text{Mn}_5\text{O}_5$ | 10 | 1 | 2.6 [this work] | |

(for instance $\text{Ca}_2\text{Fe}_2\text{O}_5$ in this work) as cathodes in Ca-based batteries.

Acknowledgments

Funding from the European Union's Horizon 2020 research and innovation programme H2020 FETOPEN-1-2016-2017 (CARBAT, grant agreement no. 766617) is acknowledged. The authors are grateful for

access to the computational facilities from Universidad de Oviedo (MALTA-Consolider cluster) and the Spanish.

References

- J. Muldoon, C.B. Bucur, T. Gregory, Quest for nonaqueous multivalent secondary batteries: magnesium and beyond, *Chem. Rev.* 114 (2014) 11683–11720.
- A.L. Lipson, B. Pan, S.H. Lapidus, C. Liao, J.Y. Vaughney, B.J. Ingram, Rechargeable Ca-ion batteries: a new energy storage system, *Chem. Mater.* 27 (2015) 8442–8447.
- R.J. Gummow, G. Vamvounis, M.B. Kannan, Y. He, Calcium-ion batteries: current state-of-the-art and future perspectives, *Adv. Mater.* 30 (2018), e1801702.
- A. Ponrouch, M.R. Palacin, On the road toward calcium-based batteries, *Curr. Opin. Electrochem.* 9 (2018) 1–7.
- A. Ponrouch, C. Frontera, F. Barde, M.R. Palacin, Towards a calcium-based rechargeable battery, *Nat. Mater.* 15 (2015) 169–172.
- D. Wang, X. Gao, Y. Chen, L. Jin, C. Kuss, P.G. Bruce, Plating and stripping calcium in an organic electrolyte, *Nat. Mater.* 17 (2018) 16–20.
- P. Canepa, G.S. Gautam, D.C. Hannah, R. Malik, M. Liu, K.G. Gallagher, K.A. Persson, G. Ceder, Odyssey of multivalent cathode materials: open questions and future challenges, *Chem. Rev.* 117 (2017) 4287–4341.
- D.S. Tchitchevka, A. Ponrouch, R. Verrelli, T. Broux, C. Frontera, A. Sorrentino, F. Barde, N. Biskup, M.E. Arroyo-de Dompablo, M.R. Palacin, Electrochemical intercalation of calcium and magnesium in TiS_2 : fundamental studies related to multivalent battery applications, *Chem. Mater.* 30 (2018) 847–856.
- M. Cabello, F. Nacimiento, R. Alcantara, P. Lavela, C. Pérez-Vicente, J.L. Tirado, Applicability of molybdate as an electrode material in calcium batteries: a structural study of layer-type Ca_3MoO_6 , *Chem. Mater.* 30 (2018) 5853–5861.
- M. Cabello, F. Nacimiento, J.R. González, G. Ortiz, R. Alcantara, P. Lavela, C. Pérez-Vicente, J.L. Tirado, Advancing towards a veritable calcium-ion battery: CaCo_2O_4 positive electrode material, *Electrochim. Commun.* 67 (2016) 59–64.
- Y.S. Meng, M.E. Arroyo-de Dompablo, Recent advances in first principles computational research of cathode materials for lithium-ion batteries, *Accounts Chem. Res.* 46 (2013) 1171–1180.
- M. Liu, Z. Rong, R. Malik, P. Canepa, A. Jain, G. Ceder, K.A. Persson, Spinel compounds as multivalent battery cathodes: a systematic evaluation based on *ab initio* calculations, *Energy Environ. Sci.* 8 (2015) 964–974.
- M. Liu, A. Jain, Z. Rong, X. Qu, P. Canepa, R. Malik, G. Ceder, K.A. Persson, Evaluation of sulfur spinel compounds for multivalent battery cathode applications, *Energy Environ. Sci.* 9 (2016) 3201–3209.
- M.E. Arroyo-de Dompablo, C. Krich, J. Nava-Avendaño, N. Biskup, M. Rosa Palacin, F. Barde, A joint computational and experimental evaluation of CaMn_2O_4 polymorphs as cathode materials for Ca ion batteries, *Chem. Mater.* 28 (2016) 6886–6893.
- M.E. Arroyo-de Dompablo, C. Krich, J. Nava-Avendaño, M.R. Palacín, F. Bardé, In quest of cathode materials for ca ion batteries: the CaMO_3 perovskites ($M = \text{Mo, Cr, Mn, Fe, Co, Ni}$), *Phys. Chem. Chem. Phys.* 18 (2016) 19966–19972.
- Z. Rong, R. Malik, P. Canepa, G.S. Gautam, M. Liu, A. Jain, K. Persson, G. Ceder, Materials design rules for multivalent ion mobility in intercalation structures, *Chem. Mater.* 27 (2015) 6016–6021.
- G.S. Gautam, P. Canepa, R. Malik, M. Liu, K. Persson, G. Ceder, First-principles evaluation of multi-valent cation insertion into orthorhombic V_2O_5 , *Chem. Commun.* 51 (2015) 13619–13622.
- P. Millet, C. Satto, P. Sciau, J. Galy, MgV_2O_5 and $8\text{Li}_x\text{V}_2\text{O}_5$: a comparative structural investigation, *J. Solid State Chem.* 136 (1998) 56–62.
- R. Verrelli, A.P. Black, C. Panathanummasid, D.S. Tchitchevka, A. Ponrouch, J. Oro-Sole, C. Frontera, F. Barde, P. Rozier, M.R. Palacin, On the strange case of divalent ions intercalation in V_2O_5 , *J. Power Sources* 407 (2018) 162–172.
- D.S. Tchitchevka, C. Frontera, A. Ponrouch, C. Krich, F. Barde, M.R. Palacin, Electrochemical calcium extraction from 1D- $\text{Ca}_3\text{Co}_2\text{O}_6$, *Dalton Trans.* 47 (2018) 11298–11302.
- D. Morgan, A. Van der Ven, G. Ceder, Li conductivity in Li_xMPO_4 ($M = \text{Mn, Fe, Co, Ni}$) olivine materials, *Electrochim. Solid State Lett.* 7 (2004) A30–A32.
- C. Ling, F. Mizuno, Phase stability of post-spinel compound AMn_2O_4 ($A = \text{Li, Na, or Mg}$) and its application as a rechargeable battery cathode, *Chem. Mater.* 25 (2013) 3062–3071.
- J. Kim, X. Yin, K.C. Tsao, S. Fang, H. Yang, $\text{Ca}_2\text{Mn}_2\text{O}_5$ as oxygen-deficient perovskite electrocatalyst for oxygen evolution reaction, *J. Am. Chem. Soc.* 136 (2014) 14646–14649.
- J.R. Petrie, H. Jeen, S.C. Barron, T.L. Meyer, H.N. Lee, Enhancing perovskite electrocatalysis through strain tuning of the oxygen deficiency, *J. Am. Chem. Soc.* 138 (2016) 7252–7255.
- Y. Zhu, W. Zhou, J. Yu, Y. Chen, M. Liu, Z. Shao, Enhancing electrocatalytic activity of perovskite oxides by tuning cation deficiency for oxygen reduction and evolution reactions, *Chem. Mater.* 28 (2016) 1691–1697.
- N. Tyminska, G. Wu, M. Dupuis, Water oxidation on oxygen-deficient barium titanate: a first-principles study, *J. Phys. Chem. C* 121 (2017) 8378–8389.
- C.A.J. Fisher, M.S. Islam, Defect, protons and conductivity in brownmillerite-structured $\text{Ba}_2\text{In}_2\text{O}_5$, *Solid State Ionics* 118 (1999) 355–363.
- N. Sharma, K.M. Shaju, G.V. Subba Rao, B.V.R. Chowdari, Mixed oxides $\text{Ca}_2\text{Fe}_2\text{O}_5$ and $\text{Ca}_2\text{Co}_2\text{O}_5$ as anode materials for Li-ion batteries, *Electrochim. Acta* 49 (2014) 1035–1043.
- J. Berggren, Refinement of crystal structure of dicalcium ferrite, $\text{Ca}_2\text{Fe}_2\text{O}_5$, *Acta Chem. Scand.* 25 (1971) 3616–3624.
- P. Berastegui, S.G. Eriksson, S. Hull, A neutron diffraction study of the temperature dependence of $\text{Ca}_2\text{Fe}_2\text{O}_5$, *Mater. Res. Bull.* 34 (1999) 303–314.

- [31] K.R. Poeppelmeier, M.E. Leonowicz, J.M. Longo, $\text{CaMnO}_{2.5}$ and $\text{Ca}_2\text{MnO}_{3.5}$: new oxygen-defect perovskite-type oxides, *J. Solid State Chem.* 44 (1982) 89–98.
- [32] M.T. Anderson, J.T. Vaughan, K.R. Poeppelmeier, Structural similarities among oxygen-deficient perovskites, *Chem. Mater.* 5 (1993) 151–165.
- [33] K.R. Poeppelmeier, M.E. Leonowicz, J.C. Scanlon, J.M. Longo, W.B. Yelon, Structure determination of CaMnO_3 and $\text{CaMnO}_{2.5}$ by x-ray and neutron methods, *J. Solid State Chem.* 45 (1982) 71–79.
- [34] C.D. Ling, J.J. Neumeier, D.N. Argyriou, Observation of antiferromagnetism in marokite CaMn_2O_4 , *J. Solid State Chem.* 160 (2001) 167–173.
- [35] J. Hadermann, A.M. Abakumov, L.J. Gillie, C. Martin, M. Hervieu, Coupled cation and charge ordering in the CaMn_3O_6 tunnel structure, *Chem. Mater.* 18 (2006) 5530–5536.
- [36] M.M. Najafpour, D.J. Sedigh, Water oxidation by manganese oxides, a new step towards a complete picture: simplicity is the ultimate sophistication, *Dalton Trans.* 42 (2013) 12173–12178.
- [37] W.S. Glaunsinger, H.S. Horowitz, J.M. Longo, A. Chang, Magnetic-properties of the mixed-valence compounds CaMn_3O_6 and CaMn_4O_8 , *J. Solid State Chem.* 35 (1980) 187–191.
- [38] N. Barrier, C. Michel, A. Maignan, M. Hervieu, B. Raveau, CaMn_4O_8 , a mixed valence manganite with an original tunnel structure, *J. Mater. Chem.* 15 (2005) 386–393.
- [39] G. Kresse, J. Furthmuller, Efficient iterative schemes for *ab initio* total-energy calculations using a plane-wave basis set, *Phys. Rev. B* 54 (1996) 11169.
- [40] J.P. Perdew, K. Burke, M. Ernzerhof, Generalized gradient approximation made simple, *Phys. Rev. Lett.* 77 (1996) 3865–3868.
- [41] P.E. Bloch, Projector augmented-wave method, *Phys. Rev. B* 50 (1994) 17953.
- [42] M.K. Aydinol, A.F. Kohan, G. Ceder, K. Cho, J. Joannopoulos, *Ab initio* study of lithium intercalation in metal oxides and metal dichalcogenides, *Phys. Rev. B* 56 (1997) 1354–1365.
- [43] A. Torres, M.E. Arroyo-de Dompablo, Comparative investigation of MgMnSiO_4 and olivine-type MgMnSiS_4 as cathode materials for Mg batteries, *J. Phys. Chem. C* 122 (2018) 9356–9362.
- [44] R.D. Shannon, C.T. Prewitt, Revised effective ionic radii in halides and chalcogenides, *Acta Crystallogr.* 32 (1976) 751–767.
- [45] J.P. Hodges, S. Short, J.D. Jorgensen, X. Xiong, B. Dabrowski, S.M. Mini, C.W. Kimball, Evolution of oxygen-vacancy ordered crystal structures in the perovskite series $\text{Sr}_n\text{Fe}_n\text{O}_{3n-1}$ ($n=2, 4, 8$, and infinity), and the relationship to electronic and magnetic properties, *J. Solid State Chem.* 151 (2000) 190–209.
- [46] R.E. Schaak, T.E. Mallouk, Perovskites by design: a toolbox of solid-state reactions, *Chem. Mater.* 14 (2002) 1455–1471.
- [47] J. Carrasco, Role of Van der Waals forces in thermodynamics and kinetics of layered transition metal oxide electrodes: alkali and alkaline-earth ion insertion into V_2O_5 , *J. Phys. Chem. C* 118 (2014) 19599–19607.